metals

MDPI

Review

A Review on Shape Memory Alloys with Martensitic Transition at Cryogenic Temperatures

Adelaide Nespoli *, Davide Ninarello and Carlo Fanciulli

Consiglio Nazionale delle Ricerche—Istituto di Chimica della Materia Condensata e di Tecnologie per l'Energia (CNR-ICMATE), via G. Previati 1/e, 23900 Lecco, Italy; davide.ninarello@icmate.cnr.it (D.N.); carlo.fanciulli@cnr.it (C.F.)

* Correspondence: adelaide.nespoli@cnr.it or adelaide.nespoli@icmate.it

Abstract: Shape memory alloys (SMA) are functional materials known for their shape memory and pseudoelastic properties, which originated from a thermoelastic phase transition between two solid phases: austenite and martensite. The ranges of temperature at which austenite and martensite are stable depend primarily on the chemical composition and the thermomechanical history of the alloy. This work presents a broad overview of shape memory alloys presenting the thermoelastic phase transition at cryogenic temperatures—that is, at temperatures below the freezing point of water. Currently, this class of SMA is not very well explored due to the difficulties in conducting both structural and functional experimentations at very low temperatures. However, these materials are of great importance for extreme environments such as space. In this work, the different classes of cryogenic SMA will first be presented as a function of their phase transformation temperatures. Hints of their mechanical performance will also be reported. Cu-based systems have been identified as cryogenic SMA presenting the lowest phase transformation temperatures. The lowest measured M_s (45 K) was found for the Cu-8.8Al-13.1Mn (wt.%) alloy.

Keywords: shape memory alloys; cryogenic environment; phase transformation temperature; martensitic transition

check for updates

Citation: Nespoli, A.; Ninarello, D.; Fanciulli, C. A Review on Shape Memory Alloys with Martensitic Transition at Cryogenic Temperatures. *Metals* **2023**, *13*, 1311. https://doi.org/10.3390/met13071311

Academic Editors: Alexander V. Shelyakov and Matthias Bönisch

Received: 28 June 2023
Revised: 13 July 2023
Accepted: 20 July 2023
Published: 21 July 2023

Copyright: © 2023 by the authors. Licensee MDPI, Basel, Switzerland. This article is an open access article distributed under the terms and conditions of the Creative Commons Attribution (CC BY) license (https://creativecommons.org/licenses/by/4.0/).

1. Introduction

Shape memory alloys (SMA) are a well-known class of structural and functional materials able to recover high deformations thanks to a solid-to-solid reversible thermoelastic martensitic transition (TMT) from a high-temperature phase, austenite, which is characterized by a cubic (bcc or B2) microstructure, to a low-temperature phase, martensite, which can have a tetragonal, orthorhombic, or a monoclinic structure. Martensite appears as multivariant (twinned), and it is characterized by a low elastic modulus and a high degree of deformability. The austenite-to-martensite TMT is identified by the M_s and M_f temperatures, which denote the temperature range in which martensite nucleates and growths from austenite. On the other hand, the martensite-to-austenite reverse TMT is identified by A_s and A_f, which are the temperatures at which the transition of the martensite into the austenite phase starts and finishes, respectively [1].

The driving force of the TMT can be either a change of temperature or a change of load. In the former case, a load-free condition does not generate a macroscopic change of shape during austenite-to-martensite transformation. Instead, under suitable loading conditions, the temperature variation promotes a macroscopic shape change from the deformed martensite to the parent austenite. In this case, we are referring to the so-called shape memory effect (SME). The mechanical work that results from SME is exploited in engineering applications to produce motion in actuators [2–5].

The second macroscopic shape recovery is related to pseudoelasticity (PE). When the shape memory material is at a temperature above A_f, the driving force of TMT is the load. During loading, the austenite behaves like a common elastic material at low strains.

When a critical stress is reached, the alloy transforms into martensite, producing high deformations and maintaining the stress constant (plateau phase). Once all the martensite is detwinned (with the prevalence of only one variant), the common linear elastic behavior of the martensite occurs. Above A_f, martensite can appear only stress-induced (SIM). Due to the instability of SIM at these temperatures, upon unloading, the reverse transformation occurs, and the lattice returns to the austenitic parent phase. This phenomenon leads to the recovery of the strain and, as a consequence, to a stress–strain closed loop. This means that PE is a reversible, non-linear elastic phenomenon. However, the pseudoelastic range is limited. It has lower bounds defined by both A_f and the critical stress to induce martensite, and an upper limit given by the critical stress to induce slip, i.e., irreversible phenomena. The mechanical energy dissipated during a load–unload cycle finds numerous applications in passive damping to prevent permanent damage to structures and equipment [6–8].

The temperature range of stability of the two phases depends on the chemical composition of the alloy and on the metallurgical condition the material was subjected to before the final use, such as the mechanical processing and the thermal treatments. However, in designing an application, it should be kept in mind that the phase transformation temperatures are also strictly related to the environmental temperature and the applied load (Clausius–Clapeyron law, [1]). As a result, operating constraints such as temperature, applied load, deformation range, and life cycle guide the designer in the selection of the SMA material.

Common uses of SMA involve NiTi, NiTi-based and Cu-based alloys and are taken at a temperature that spans from room temperature (PE) to approximately 400 K for typical SME alloys or up to approximately 600 K for high temperature SMA, such as NiTiHf [1,9]. The main uses are medicine (such as stents, grafts, orthopedic staples, orthodontic archwires, eyeglass frames), aerospace and military (such as couplers in F14 planes), safety (such as dampers of seismic vibrations and sprinklers), and robotics (such as actuators) [10–14].

The control—either active or passive—of structures at very-low temperatures through SMA represents an attractive application for extreme environments such as space. Systems such as expandable habitats and deployable platforms, solar cells and veils, and on demand and adaptive applications, as well as ISRU (in situ resource utilization) technologies, optical mountings, and cryogenic equipment for space explorations can benefit greatly from those SMA presenting TMT in cryogenic environment.

This work aims to present a detailed overview of the main SMA with TMT at cryogenic environment temperatures. We decided to select the phase transformation temperatures as the main criterion used to identify a cryogenic SMA, with these temperatures being the most representative characteristic of these materials. As a matter of fact, only a few of the presented works also exposed a mechanical characterization of the alloys. Furthermore, among the transformation temperatures, M_s is the one most considered in the literature, being the easiest detect, even at very low temperature, with techniques such as the electrical resistance measurement equipped with helium gas. Alternatively, the most common differential scanning calorimetry equipped with nitrogen is not able to detect phase transformation temperatures below the nitrogen evaporation temperature.

Therefore, in the present work, we considered cryogenic the SMA presenting M_s lower than 250 K and, when declared, A_f lower than 273 K. The alloys that respect these requirements are analyzed with respect to their weight composition and the TMT temperature window.

The SMA families that satisfy the above-mentioned criterion discussed in the present work belong to the NiTi-based, Cu-based, Ag-based, FePt, Magnetic SMA, and CaFeAs groups.

2. Cu-Based Systems

Within the cryogenic SMA, the Cu-based alloys are the most studied, with the CuAlMn and CuAlMn-based systems being the main families. Besides them, few works based on the CuZn and CuAl alloys can also be found. To the best of the authors' knowledge, the

first cryogenic Cu-based SMA was the CuZnSi alloy that was investigated in 1974 by Tong et al. [15]. After that first study, the other works appeared later at the end of 1990s, with a prevalent focus on the CuAlMn-based systems. The most recent works are dated to 2022 and are focused on the ternary CuAlMn alloy [16,17].

2.1. CuAlMn and CuAlMn-Based Systems

Zak et al. [18] investigated the phase transformation temperatures and the tensile mechanical response of CuAlMn wires solubilized at 1123 K for 15 min and air cooled down to room temperature. The effect of the chemical composition on the phase transformation temperature was evaluated considering Mn content approximately equal to 11 and 12 wt.% and Al content in the range from 8 to 9.5 wt.%. Within the considered Mn and Al ranges, the lowest phase transformation temperatures were identified for the Cu-8.9Al-12Mn (wt.%) alloy (92 K for M_s and 123 K for A_f). Furthermore, this alloy exhibited 7% shape recovery and 5% pseudoelastic strain.

Other interesting studies include those of Prado et al. [19], Bubley et al. [20], and Omori et al. [21]. Prado et al., reported for the Cu-8.7Al-10.8Mn (wt.%) and Cu-8.5Al-11.7Mn (wt.%) systems an M_s value of 161 K and 82 K, respectively. Bubley et al., investigated a family of CuAlMn systems with Al ranging from 12 to 14 wt.% and Mn from 2 to 10 wt.%. Samples were solubilized and then aged at 523 K. The lowest M_s temperature was found equal to 93 K for Cu-14Al-6Mn (wt.%). The other three alloys presented close M_s: 108 K, 123 K. and 133 K, respectively, for Cu-13Al-8Mn (wt.%), Cu-12Al-10Mn (wt.%), and Cu-14Al-4Mn (wt.%). Finally, Omori et al., studied different CuAlMn systems and found the lowest M_s temperature (111 K) when Al and Mn content were, respectively, 8.2 and 12.7 wt.%.

Shajil et al. [22] explored the quaternary CuAlMnNi and CuAlMnCo systems. The selected alloy compositions were Cu-8Al-9.5Mn-2.1Ni and Cu-8.1Al-10.2Mn-0.5Co (wt.%). These two alloys were hot worked down to strips and thermal treated: first at 1203 K for 8 min, followed by water quenching; and second at 473 K for 15 min, followed by air cooling. After the thermomechanical route, the CuAlMnNi and CuAlMnCo alloys display a TMT at low temperatures with M_s at 211 and 213 K, respectively. The respective A_f were 230 and 232 K. Cyclic tests resulted in a dissipation energy in the order of 1–1.7MJ/m^3/cycle at large strain amplitude.

Niitsu et al. [23] studied the effects of annealing on the PE response at 77 K of a CuMnAl alloy rod (Cu-8.2Al-14.7Mn, wt.%). In a subsequent work, they also investigated single crystal plates of CuAlMn alloy (Cu-8.2Al-14.7Mn and Cu-8.2Al-11.7Mn, wt.%) finding a PE response in the range from 4.2 K to 160 K (for annealed samples) [24].

Investigating the elastocaloric effect of a single crystal of Cu-7.1Al-11.6Mn (wt.%), Qian et al. [25] found an M_s temperature of 234 K. Furthermore, compression tests at room temperature showed 120 MPa stress at the maximum recoverable strain of 4.0% and a 3.9 K adiabatic temperature change. Liu et al. [26] investigated the pseudoelasticity and the bainite plates precipitation with aging of the Cu-8.6Al-10.8Mn (wt.%) alloy. The columnar grained ingot presented an M_s of 225 K.

An analysis of the behavior of the CuAlMn alloy was also proposed by Lei et al. [27], who found a martensite start temperature of 120 K in CuAlMn (Cu-11.3Al-9.4Mn, wt.%) through an in situ observation of the martensitic transformation. Based on this work, the same research group recently studied the martensitic transformation of another cryogenic CuAlMn alloy (Cu-12.5Al-10.7Mn, wt.%) with a martensite start temperature of 108 K [17]. This study came to the conclusion that the austenite phase could transform in several martensite variants, but all of them will transform back to the same austenite during the reverse transformation, both under null and non-zero compressive stress. Furthermore, they found that the martensitic transformation is not complete, as a little percentage of austenite phase remains.

Interest in the CuAlMn system was also showed by Wang et al. [28]. In particular, they reported on a cryogenic system (Cu-8.8Al-13.1Mn, wt.%) with M_s and A_f temperatures,

respectively, of 45 and 85 K. However, a low elastic modulus of 30 GPa was obtained. They also discussed the correlation between martensite temperature and the content of Al and Mn, concluding that a linear relationship between M_s and the content of Al and Mn exists. The linear dependency was then expressed in the form of the equation reported in Table 1.

Table 1. M_s formulae for the CuAlMn alloy [18,28,29].

Relationship	Al Range	Mn Range	Reference
M_s(K) = 1192 − 25.5Al(wt.%) − 73.2Mn(wt.%)	8–9.5 wt.%	10.9–12 wt.%	[18]
M_s (K) = 1890 − 42.1Al(at.%) − 78Mn(at.%)	17.7–18.1 at.%	11.4–13.3 at.%	[28]
M_s (K) = 1983 − 127.4Al(wt.%) − 43.6Mn(wt.%)	10–11 wt.%	5–7.5 wt.%	[29]
M_s (K) = 2129 − 63.2Al(at.%) − 63.9Mn(at.%)	20–25 at.%	5–10 at.%	[29]

Recently, Trehern et al. [16] presented a comprehensive investigation of the cryogenic CuAlMn alloy through a study on the thermomechanical functionality for several compositions. They showed that the phase transformation temperatures of this system can be drastically decreased by opportunely changing the Mn/Al ratio. They reported that an increase of 1 at.% in Mn causes a temperature drop of 74 K, a result in agreement with what was found by Zak et al. [18]. The lowest phase transformation temperatures were found for the alloy with a measured composition of Cu-9.2Al-12.4Mn (wt.%). For this composition, the M_s and A_f temperatures were 70 K and 91 K, respectively. Furthermore, Trehern et al., for the first time, investigated the thermomechanical functionality of CuAlMn SMA and obtained a maximum recoverable actuation strain of 3.05% under 250 MPa at low temperatures. In low temperature actuation, CuAlMn withstands significant stress levels and yields higher actuation strains than previously studied CuAlMn alloys with transition temperatures higher than 273 K. Additionally, fully recoverable 1.81% and 2% superelastic strains were obtained at temperatures as low as 133 K and 173 K, respectively.

Figure 1 collects the data of the analyzed papers, focusing attention on M_s temperature as a function of the Mn content (Figure 1a) and the Mn/Al ratio (Figure 1b). In the two graphs, data were divided into three main groups according to the content of Al, from 8 to 8.9 wt.% (blue color), from 9 to 9.4 wt.% (green color), and from 12 to 14 wt.% (orange color). In addition, the data were divided into two sub-groups according to the heat treatment considered for each material: solubilization (light color) or solubilization followed by annealing (dark color). In Figure 1a, it can be noted that for Mn higher than 10 wt.% and Al in the range from 8 to 9.4 wt.%, a little increase in Mn content enables a fast decrease in M_s. On the other hand, for Mn content lower than 10 wt.% and Al in the range from 12 to 14 wt.%, M_s does not show a significant variation with the increasing of Mn content. Considering the Mn/Al ratio (Figure 1b), the two trends just described are identified by the two regions visible for Mn/Al ratio lower and higher than 1.

The strong effect of the chemical composition on the transformation temperatures of the CuAlMn alloy has been identified and studied in the past by many authors. In particular, four main relationships were identified to assess the martensite start temperature (M_s) in specific Al and Mn ranges, as reported in the work of Zak et al., Wang et al., and Zheng et al. [18,28,29] (see Table 1).

According to these formulae, four theoretical regions in the M_s vs. Mn content diagram can be recognized (see the colored regions in the diagram of Figure 2). The diagram shows some data that are partially outside the limit of the present study, i.e., alloys with M_s higher than 250 K. However, they confirm the trend observed for the cryogenic materials. M_s transition temperature decreases with the very slight increase in the weight percentage of Al and Mn content. The highest variation is particularly given for Mn content lower than 10 wt.%. In this region, M_s is related mostly to Al content: the increase of 1 wt.% of Al content allows a temperature drop of more than 100 K. On the other side, for Mn content higher than 10 wt.%, the M_s trend depends mostly on Mn.

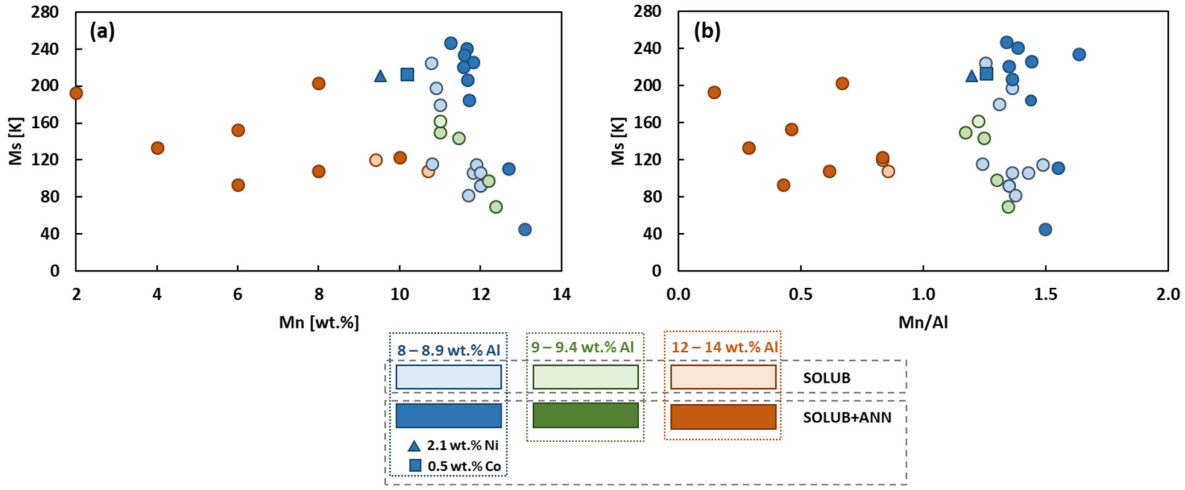


Figure 1. M_s as a function of Mn content (**a**), and as a function of the Mn/Al ratio (**b**), of CuAlMn-based cryogenic SMA: blue color: 8–8.9 wt.% Al; green color: 9–9.4 wt.% Al; orange color: 12–14 wt.% Al. Materials followed solubilization (light colors) or solubilization followed by annealing, (dark colors).

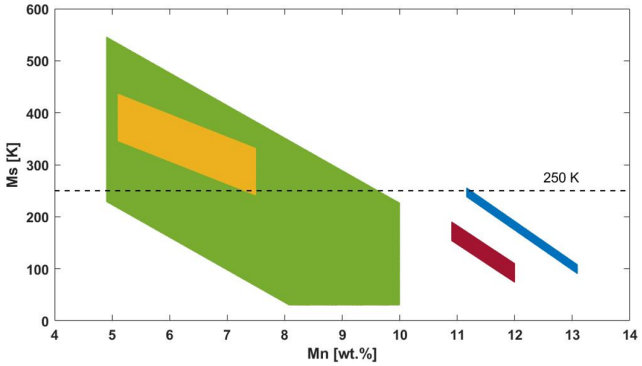


Figure 2. M_s as a function of Mn content with evidence of the four regions identified by ref. [18] (dark red color), ref. [28] (blue color), ref. [29] (green and orange colors). The dashed line represents the M_s limit below which the material can be considered cryogenic.

Finally, Figures 1 and 2 suggest that the explored areas in which the material show M_s at cryogenic level are very few and narrow, providing an opportunity for further investigations. In particular, Figure 1 advises new studies focused on obtaining lower M_s to consider Mn content higher than 13 wt.%, Al content lower than 8 wt.%, and Mn/Al ratio higher than 1.5.

2.2. CuZn-Based and CuAl-Based Alloys

Investigations on the CuZn-based alloy were first accomplished by Tong et al. [15]. They reported for the Cu-36.8Zn-0.6Si alloy an M_s of 218 K after annealing. More recently, Qian et al. [25] investigated the elastocaloric property of an annealed polycrystalline CuZnAl with a composition of Cu-18Zn-7.4Al. For this alloy, they measured M_s and A_f temperatures of 219 and 234 K, respectively. Malarría et al. [30] studied single-crystal CuZnAl alloys with different tensile axis orientations to determine the contribution of each mechanic and/or defect to the two-way shape memory effect (TWSME). Three main alloys concentrations were considered: Cu-21.1Zn-6.7Al (wt.%), Cu-22Zn-6.5Al (wt.%), and Cu-22.8Zn-6.3Al (wt.%). The lowest M_s values within the three subgroups were 146 K, 152 K, and 135 K, respectively.

Among the possible ternary additions to these Cu-SMA main subgroups, Be presents great advantages inasmuch as CuAlBe offers interesting mechanical and physical proper-

ties [31]. Furthermore, the addition of Be to the alloy leads to a reduction in the M_s. For example, Belkahla et al. [32] studied the effect of Be and Al content on CuAlBe alloys and found that Be is most effective in decreasing M_s. In particular, varying the Be content in the range from 0.3 to 0.65 wt.% in Cu-11.7Al-Be (wt.%), they found that M_s decreases at the rate of 893 ± 20 K per wt.% of Be. This rate is almost 12 times higher than the effect of Al content variation for Cu-Al-0.47Be (wt.%), with the Al content ranging between 10 and 12.5 wt.%. The two alloys with the lowest M_s were Cu-12.5Al-0.47Be and Cu-11.7Al-0.65Be with, respectively, 213 K and 128 K. Finally, for weight content of Al and Be ranging from 10 to 12.5 wt.% and from 0.3 and 0.65 wt.%, respectively, they determined the following relationship between M_s and the elements content:

$$M_s(K) = 1518 - 71Al(wt.\%) - 893Be(wt.\%). \quad (1)$$

Other researchers focused on CuAlBe with different element concentrations. In particular, Higuchi et al. [33] found M_s equal to 250 K and 241 K for, respectively, Cu-9.55Al-0.86Be (wt.%) and Cu-11.46Al-0.59Be (wt.%). They also analyzed internal friction and electric resistivity as a function of temperature, determining the peak of internal friction near the transformation temperature of the alloy. Furthermore, they noticed an increase in the peak value of internal friction with an increase in Al content, together with a reduction in the Young's modulus. Similarly, Zuñiga et al. [34] studied CuAlBe systems to demonstrate the good TWSME under bending. They studied a Cu-11.9 wt.%. andAl-0.5 wt.% Be with M_s equal to 231 K and determined a decrease in the TWSME strain with the number of thermal cycles, observing the main loss within the first 30 cycles.

It is also worth highlighting the work of Rios-Jara et al. [35], which tried to relate the thermodynamic and elastic properties of CuAlBe shape memory alloys. To do so, they analyzed five different alloys with Al and Be ranging, respectively, from 11.50 to 11.79 wt.% and from 0.47 and 0.6 wt.%. Among them, three alloys presented TMT at cryogenic temperatures. In particular, they found an M_s equal to 240, 221, and 153 K for, respectively, Cu-11.63Al-0.5Be (wt.%), Cu-11.79Al-0.54Be (wt.%), and Cu-11.50Al-0.6Be (wt.%).

With respect to the CuAlMn-based alloys, the data available for the CuZn- and CuAl-based systems are limited, and an investigation for wider range of compositions is missing. The M_s dependence by the alloy composition in the investigated range turns out to be linear as already observed for CuAlMn. Here, again, a relevant change in phase transition temperature is driven by a narrow range of alloy compositions.

Table 2 summarizes the Cu-based SMA, presenting the TMT at cryogenic temperatures. The table lists the M_s and A_f temperatures as well as the thermal treatment (TT) followed by each alloy.

Table 2. Cu-based cryogenic SMA ordered according to M_s value (TT: thermal treatment; S: solubilized; A: annealed; ND: not declared; REF.: reference).

Cu [wt.%]	Al [wt.%]	Mn [wt.%]	Ni [wt.%]	Co [wt.%]	Zn [wt.%]	Si [wt.%]	Be [wt.%]	M_s [K]	A_f [K]	TT	REF.
78.1	8.8	13.1	-	-	-	-	-	45	85	A	[28]
78.4	9.2	12.4	-	-	-	-	-	70	91	S	[16]
79.8	8.5	11.7	-	-	-	-	-	82	ND	S	[19]
79.1	8.9	12	-	-	-	-	-	92	123	S	[18]
80	14	6	-	-	-	-	-	93	ND	A	[20]
78.4	9.4	12.2	-	-	-	-	-	98	116	S	[16]
79.5	8.7	11.8	-	-	-	-	-	106	122	S	[16]
79.6	8.4	12	-	-	-	-	-	106	137	S	[18]
79	13	8	-	-	-	-	-	108	ND	A	[20]

Table 2. *Cont.*

Cu [wt.%]	Al [wt.%]	Mn [wt.%]	Ni [wt.%]	Co [wt.%]	Zn [wt.%]	Si [wt.%]	Be [wt.%]	M_s [K]	A_f [K]	TT	REF.
76.8	12.5	10.7	-	-	-	-	-	108	145	S	[17]
79.1	8.2	12.7	-	-	-	-	-	111	ND	A	[21]
80.1	8	11.9	-	-	-	-	-	115	143	S	[18]
79.3	11.3	9.4	-	-	-	-	-	120	ND	S	[27]
78	12	10	-	-	-	-	-	123	ND	A	[20]
87.6	11.7	-	-	-	-	-	0.6	128	ND	S	[32]
82	14	4	-	-	-	-	-	133	ND	A	[20]
70.9	6.3	-	-	-	22.8	-	-	135	ND	A	[30]
79.3	9.2	11.5	-	-	-	-	-	144	157	S	[16]
72.2	6.7	-	-	-	21.1	-	-	146	ND	A	[30]
79.6	9.4	11	-	-	-	-	-	150	183	S	[18]
71.5	6.5	-	-	-	22	-	-	152	ND	A	[30]
87.9	11.5	-	-	-	-	-	0.6	153	152	ND	[35]
81	13	6	-	-	-	-	-	153	ND	A	[20]
80.5	8.7	10.8	-	-	-	-	-	161	ND	S	[19]
80	9	11	-	-	-	-	-	162	203	S	[18]
80.6	8.4	11	-	-	-	-	-	180	218	S	[18]
80.2	8.1	11.7	-	-	-	-	-	185	ND	A	[21]
84	14	2	-	-	-	-	-	193	ND	A	[20]
81.1	8	10.9	-	-	-	-	-	198	230	S	[18]
80	12	8	-	-	-	-	-	203	ND	A	[20]
79.7	8.6	11.7	-	-	-	-	-	207	224	A	[28]
80.4	8	9.5	2.1	-	-	-	-	211	230	A	[22]
81.2	8.1	10.2	-	0.5	-	-	-	213	232	A	[22]
87.03	12.5	-	-	-	-	-	0.47	213	ND	S	[32]
62.6	-	-	-	-	36.8	0.6	-	218	ND	A	[15]
74.5	7.4	-	-	-	18	-	-	219	234	A	[25]
87.67	11.79	-	-	-	-	-	0.54	221	219	ND	[35]
79.8	8.6	11.6	-	-	-	-	-	221	234	A	[28]
80.6	8.6	10.8	-	-	-	-	-	225	237	S	[26]
80.0	8.2	11.8	-	-	-	-	-	226	243	A	[28]
87.6	11.9	-	-	-	-	-	0.5	231	253	S	[34]
81.3	7.1	11.6	-	-	-	-	-	234	261	S	[25]
87.87	11.63	-	-	-	-	-	0.50	240	238	ND	[35]
87.95	11.46	-	-	-	-	-	0.59	241	ND	A	[33]
80	8.4	11.6	-	-	-	-	-	241	254	A	[28]
80.3	8.4	11.3	-	-	-	-	-	247	265	A	[28]

3. NiTi-Based Alloys

NiTi-based alloys are the most common and exploited SMA. With respect to the other alloy families, for particular thermomechanical conditions, an additional martensite

phase with a trigonal cell, called the R-phase, may also appear to generate a two-step transformation. R-phase is identified by the start and finish temperatures, R_s and R_f [1].

The addition of a third element to the binary Ni–Ti system is often used to change the phase transformation temperatures. The greater part of alloying elements lowers the transformation temperatures with respect to the Ni–Ti system (as an example Cr, Mn, Fe, V, and Co for Ni, and Al for Ti). On the other hand, adding elements such as Zr for Ti and Au, Hf, Pt, and Pd for Ni contribute to the increase in the transformation temperatures. The typical direct B2–B19′ martensitic transition of NiTi could be altered by the addition of a third element. For example, adding Fe for Ni, the alloy shows a two-stage B2–R–B19′ transformation, while with the substitution of Ni for Pd, the transformation changes into B2–B19 (B2, B19′, R, and B19 are the cubic, the monoclinic, the trigonal, and the orthorhombic structure, respectively) [1]. In the next paragraphs, ternary and quaternary NiTi-based systems are analyzed to highlight the functionality in cryogenic environment.

3.1. NiTiFe Alloys

Benafan et al. [36], based on the study of Krishnan et al. [37], took advantage of the addition of Fe in NiTi alloy to introduce the R-phase in order to reduce the transformation temperatures of the material. The considered alloy was the 51.9Ni-44.6Ti-3.5Fe (wt.%), which was then exploited to develop a helical spring actuator system to act as a thermal switch, working between the R-phase and austenite in the range from 245 K (R_f) and 267 K (A_f).

Similarly, Aaltio et al. [38] studied the R-phase transformation in two Ni–Ti–Fe alloys: 52.9Ni-45Ti-2.1Fe (wt.%) and 50.8Ni-45Ti-4.2Fe (wt.%). They found an M_s equals to 208 K for the former alloys, while for the latter, no M_s was measurable via thermal analysis. Nevertheless, the R_s temperatures were, respectively, 283 K and 232 K, in line with the results of Benafan et al. [36]. According to the limits on M_s and A_f considered in the present work, only the 50.8Ni-45Ti-4.2Fe (wt.%) could be considered cryogenic thanks to its A_f equal to 240 K. Furthermore, they determined the mechanical properties under tensile test at temperatures both higher than A_f and close to R_s, respectively. They concluded that the Young's Modulus is almost insensitive to temperature change in the R-phase, while it is strongly affected by its change in the austenite phase.

Liang et al. [39] investigated the addition of Nb and Ta on ternary NiTiFe SMA. Of particular interest is the Nb addition to the alloy (48.4Ni-46.5Ti-3.4Fe-1.7Nb, wt.%), which drastically decreases the transformation temperatures with respect to the ternary 49.8Ni-46.8Ti-3.4 Fe (wt.%). In particular, they observed an M_s and A_f, respectively, equal to 238 K and 240 K for NiTiFeNb alloy, as well as M_s equal to 261 K and A_f equal to 270 K for the ternary NiTiFe. On the other side, the addition of Ta decreases the phase transformation temperature but not to same extent as Nb, with M_s and A_f being, respectively, equal to 258 K and 267 K. Together with the thermal properties, the stress–strain curve under uniaxial compression at room temperature was also obtained for the considered alloys. They observed a higher yield strength for the quaternary alloy than the ternary one. In particular, Nb addition seemed to determine a higher strengthening of the NiTi-based SMA with respect to the addition of Ta.

3.2. Effect of Nb and Co on NiTi System

Jing et al. [40] investigated the effects of the addition of Co on the thermal and thermomechanical properties of NiTi. Within the analyzed alloys, the 46.2Ni-45Ti-8.8Co (wt.%) exhibited an M_s of approximately 140 K. Similarly, Dang et al. [41] studied the PE effect at low temperatures of Ni–Ti alloys doped with a small amount of Co atoms. The resultant alloy was 44.1Ti-49.3Ni-6.6Co (wt.%) and presented no endothermic or exothermic peak in the differential scanning calorimetry curve between 123 K and 373 K. Furthermore, through X-ray diffraction analyses, they found that the alloy remained in a single B2 structure even below 113 K, indicating a stable austenite phase at cryogenic temperatures.

Indeed, the alloy presented a fully recoverable strain, with a flag-shape stress–strain curve down to 173 K.

Furthermore, the influence of Nb addition on the TMT was thoroughly studied by Wang et al. [42], who indicated three alloys with low phase transformation temperature: 52.6Ni-39Ti-8.4Nb, 52.7Ni-39.7Ti-7.6Nb, and 48.4Ni-36.9Ti-14.7Nb (wt.%). For these alloys, M_s and A_f were 173 and 255 K, 196 and 262 K, and 200 and 262 K, respectively.

Merging the effect of Nb and Co addition to NiTi-based alloys, Sui et al. [43] investigated the effect of Co addition on the microstructure of Ni–Ti–Nb alloys. Starting from 47.9Ni-37.4Ti-14.7Nb, they analyzed both the phase transformation and mechanical properties of five alloys, keeping Ti and Nb at fixed values and adding very few atomic percentages of Co in substitution of Ni. They observed the occurrence of a one-step thermoelastic martensitic transformation both under cooling and heating (B2 $\leftrightarrow$ B19′). Furthermore, they found a decrease in M_s with while increasing of the content of Co. In particular, a TMT at cryogenic level was identified for the 45.8Ni-37.4Ti-14.7Nb-2.1Co and 46.3Ni-37.4Ti-14.7Nb-1.6Co (wt.%) alloys. The two quaternary systems presented M_f, respectively, equal to 166 and 198 K, and A_f to 228 and 263 K.

3.3. NiTiHf Alloys

Among cryogenic SMA, recent works on NiTiHf low-temperature alloys are worth highlighting. As already mentioned in the introduction section, NiTiHf systems are typically used as high-temperature shape memory alloys [9]. However, in recent years, some research groups tried to take advantage of the great properties of NiTiHf, such as its low costs, remarkable shape memory and superelasticity, and superior stability, even in low temperature applications. For example, Benafan et al. [44] evaluated the potential of NiTiHf as low-temperature SMA by mapping M_f as a function of Hf content. From their results, it is clear that for specific Hf concentrations, NiTiHf presents TMT at cryogenic level. In particular, they found M_f below 233 K for all the alloys with the exception of few samples, and the lowest M_f was found for Ti-46.9Ni-22.4Hf (wt.%), equal to 134 K, which also present an M_s equal to 166 K. For NiTiHf, Table 3 reports the alloys presenting an M_f below 233 K, when the value of M_s is not available. In addition to the transformation temperatures, they also studied the strain–temperature relationship as a function of the applied stress (uniaxial constant-force thermal cycling). They found two main trends of the transformation strain with respect to the applied stress. In particular, it was observed that for Hf content lower than 3 at.%, the transformation strain presented a peak at intermediate stress, while for higher content of Hf, the value asymptotically approaches the maximum value increasing the applied stress.

Table 3. NiTi-based cryogenic SMA ordered according to the Ni content (TT: thermal treatment; S: solubilized; A: annealed; ND: not declared; *: R_s; **: M_f; REF.: reference).

Ni [wt.%]	Ti [wt.%]	Nb [wt.%]	Co [wt.%]	Fe [wt.%]	Hf [wt.%]	Sn [wt.%]	M_s [K]	A_f [K]	TT	REF.
34.9	13.2	-	-	-	51.8	-	232	ND	S	[45]
37.8	17.3	-	-	-	44.9	-	106	ND	S	[45]
38.9	19.3	-	-	-	41.8	-	227	ND	S	[45]
39.4	40.6	-	-	-	-	20	183	242	S	[46]
44.8	28.3	-	-	-	26.9	-	207	ND	S	[45]
45.8	37.4	14.7	2.1	-	-	-	166	228	S	[43]
46.2	45	-	8.8	-	-	-	140	ND	A	[40]
46.3	37.4	14.7	1.6	-	-	-	198	263	S	[43]
46.8	32.0	-	-	-	21.2	-	201 **	ND	S	[44]

Table 3. *Cont.*

Ni [wt.%]	Ti [wt.%]	Nb [wt.%]	Co [wt.%]	Fe [wt.%]	Hf [wt.%]	Sn [wt.%]	M_s [K]	A_f [K]	TT	REF.
46.9	30.7	-	-	-	22.4	-	166	ND	S	[44]
47.3	30.3	-	-	-	22.3	-	162 **	ND	S	[44]
47.6	46.6	-	-	-	-	5.8	224	271	S	[46]
47.7	29.9	-	-	-	22.3	-	178 **	ND	S	[44]
47.8	33.5	-	-	-	18.8	-	233 **	ND	S	[44]
48.4	36.9	14.7	-	-	-	-	200	262	S	[42]
48.4	46.5	1.7	-	3.4	-	-	238	240	S	[39]
49.3	35.8	-	-	-	14.9	-	211 **	ND	S	[44]
50.8	45.0	-	-	4.2	-	-	232*	240	S	[38]
51.9	44.6	-	-	3.5	-	-	245 *	267	A	[36]
52.0	38.7	-	-	-	9.3	-	224 **	ND	S	[44]
52.6	39.0	8.4	-	-	-	-	173	255	S	[42]
52.7	39.7	7.6	-	-	-	-	196	262	S	[42]
52.8	40.8	-	-	-	6.4	-	185 **	ND	S	[44]
53.1	41.5	-	-	-	-	5.4	155	215	S	[46]
53.3	41.8	-	-	-	-	4.9	182	232	S	[46]
53.5	42.2	-	-	-	-	4.3	190	241	S	[46]
53.7	42	-	-	-	-	4.3	172	228	S	[46]
53.9	41.8	-	-	-	-	4.3	131	191	S	[46]
54.1	42.7	-	-	-	3.3	-	206	ND	S	[44]
54.1	41.1	-	-	-	4.8	-	177	ND	S	[45]

Similarly, Umale et al. [45] studied the role of the addition of Hf in substitution of Ni on the TMT of NiTiHf SMA. Among the high number of alloys considered in their work, there were several of them with TMT at cryogenic temperatures. In particular, they found M_s equal to 177, 207, 227, 106, and 232 K for, respectively, Ti-54.1Ni-4.8Hf (wt.%), Ti-44.8Ni-26.9Hf (wt.%), Ti-38.9Ni-41.8Hf (wt.%), Ti-37.8Ni-44.9Hf (wt.%), and Ti-34.9Ni-51.8Hf (wt.%). Furthermore, for Ti-50.0Ni-14.9Hf (wt.%), Ti-45.0Ni-26.9Hf (wt.%), and Ti-41.0Ni-36.7Hf (wt.%), no TMT was observed up to 13 K.

3.4. NiTiSn Alloys

Among NiTi-based SMA with TMT at cryogenic temperature, it is worth mentioning the NiTiSn alloy. Of particular interest is the study of Young et al. [46], which studied the thermal properties of several NiTiSn SMA families with the aim of producing an alloy with Af close to 123 K. In particular, they developed two main alloys that, respectively, substitute Sn for Ni (first family) and for Ti (second family). Within the first family, two alloys with TMT at cryogenic temperatures have been obtained with M_s equals to 224 and 183 K for, respectively, 47.6Ni-46.6Ti-5.8Sn and 39.4Ni-40.6Ti-20Sn (wt.%, nominal composition). Conversely, the second family did not display TMT for temperatures higher than 98 K, so no M_s has been measured. However, comparing the two families, they concluded that the substitution of Sn with Ti reduces the transformation temperatures twice as effectively. By increasing the solubilization route from 30 min to 24 h, the second family presented TMT at a cryogenic level with M_s equal to 190, 182, and 155 K for, respectively, 53.5Ni-42.2Ti-4.3Sn, 53.3Ni-41.8Ti-4.9Sn, and 53.1Ni-41.5Ti-5.4Sn (wt.%, nominal composition).

Finally, maintaining the same solubilization treatment, they found M_s equal to 172 and 131 K, respectively, for 53.7Ni-42Ti-4.3Sn and 53.9Ni-41.8Ti-4.3Sn.

Table 3 lists ternary and quaternary NiTi-based systems that present the TMT in a cryogenic environment. In particular, details on the chemical composition, M_s and A_f, as well as the thermal treatment route, are highlighted.

Figure 3 depicts the atomic content of Ni and Ti of the cryogenic NiTi-based alloys considered in the present overview. It can be noted that the greater part of the studies focused on ternary and quaternary NiTi-based systems with Ni content higher than that of Ti. Furthermore, the range of variability of Ti content within the alloys is larger than that of Ni. This suggests that the ternary and quaternary NiTi-based systems transform at ever lower temperatures when the adding elements are substituted heavily with Ti.

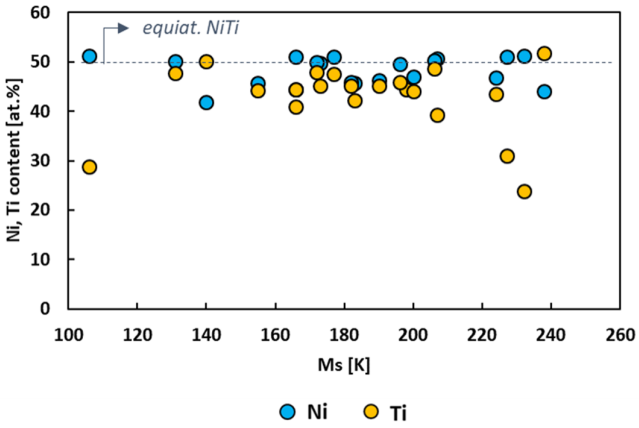


Figure 3. Ni (blue circles) and Ti (yellow circles) content (at.%) of the cryogenic NiTi-based alloys as a function of M_s.

4. Ag-Based and FePt Alloys

The first classes of SMA based on noble metals and presenting the TMT at cryogenic temperatures were the AgCd system and the FePt alloy investigated by Tong et al. [15] and the AgAl system studied by Kubo et al. [47] (see Table 4).

Table 4. Ag-based cryogenic SMA ordered according to M_s value (TT: thermal treatment; A: annealed; REF.: reference).

Ag [wt.%]	Cd [wt.%]	Al [wt.%]	M_s [K]	A_f [K]	TT	REF.
51.2	48.8	-	126	136	A	[15]
52.2	47.8	-	153	164	A	[15]
53.2	46.8	-	186	194	A	[15]
54.2	45.8	-	210	233	A	[15]
54.5	45.5	-	219	238	A	[15]
92.6	-	7.4	229	237	A	[47]

Regarding AgCd alloys, the one presenting the lowest phase transformation temperature is the 51.2Ag-48.8Cd (wt.%), which shows an M_s of 126 K and an A_f of 136 K. In the same work of Tong et al., a cryogenic TMT was also identified for the 47.5Fe-52.5Pt (wt.%) alloy which has M_s of 193 K and A_f of 208 K.

Besides this work, Kubo et al., showed the occurrence of the TMT at low temperatures in the 92.6Ag-7.4Al (wt.%) alloy, identifying the M_s at 229 K and the A_f at 237 K.

Figure 4 collects the M_s data referring to the Ag-based alloys. It can be noted that the M_s of AgCd alloy decreases linearly with the increasing of Cd. This was previously

confirmed by Tong et al. [15], who found a rate of decrease with Cd content of 30 K/at.%. Similar results were also found by Prasad et al. [48] in 1986.

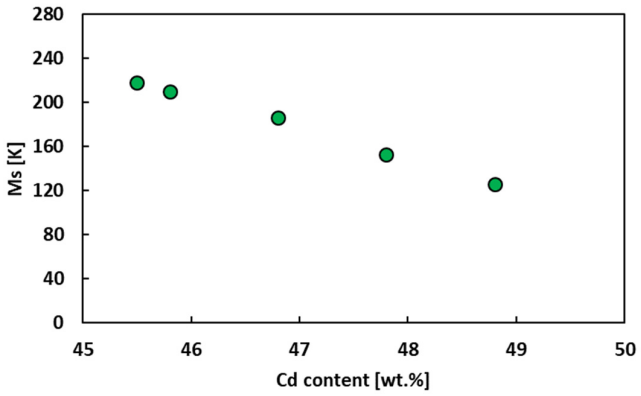


Figure 4. M_s of AgCd alloy as a function of the content of Cd.

5. $CaFe_2As_2$ Alloy

Sypek et al. [49] suggested the strong potential of $CaFe_2As_2$ alloy as a structural material in the cryogenic environment. They reported on the functional response of single-crystal micro-pillars of $CaFe_2As_2$ and showed that the material exhibits superelasticity with over 13% recoverable strain, 3 GPa yield strength, and linear shape memory effects at approximately 50 K.

6. Cryogenic Magnetic SMA

Based on stress-induced martensitic transformation, elastocaloric refrigeration of ferromagnetic SMA has been recognized as the most promising alternative solid-state refrigeration technology due to its substantial potential for energy savings. For example, Guo et al. [50] suggested the 48.4Ni-20.8Mn-28.7Ga-2.1Cu (wt.%) as a promising candidate for low-temperature elastocaloric refrigeration due to the low M_s and A_f temperature that were identified, respectively, at 218 K and 228 K.

Furthermore, a class of magnetic SMA showing a thermal transformation arrest phenomenon has been reported. This consists in an interruption of the TMT at a certain temperature (i.e., the thermal transformation arrest temperature, TA) during magnetic-field cooling, and the parent phase remains when it is cooled down to cryogenic temperatures. Taking advantage of this peculiar feature, Niitsu et al. [51] reported on the pseudoelastic response of a single crystal 35.6Ni-4Co-26.7Mn-33.7In (wt.%) in the wide range of temperature from 200 to 4.2 K.

7. Discussion

This paper presents an overview of the most relevant SMA that exhibit the TMT at cryogenic temperatures. The timeline reported in Figure 5 keeps track of the cryogenic SMA systems published within the last five decades.

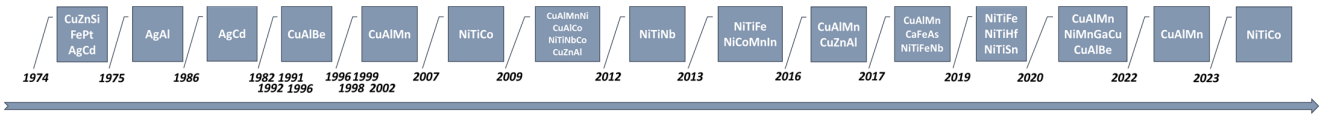


Figure 5. Timeline of the research on cryogenic SMA systems published within the last five decades.

The pie chart in Figure 6 shows the cryogenic SMA grouped according to the chemical composition. In particular, it shows the number (in percentage) of alloys studied up to now for each family considered. It can be observed that the Cu-based alloys are the most studied, and among them, the CuAlMn-based are the ones that have received the most attention. Furthermore, in accordance with the schedule in Figure 5, the CuAlMn system

has received attention since the late 1990s. The motivation behind all this focus is ascribed to their low cost, good workability, and most of all, to the temperature range at which the TMT of the CuAlMn-based alloy is located. Indeed, the CuAlMn-based systems are those presenting the lowest phase transformation temperatures.

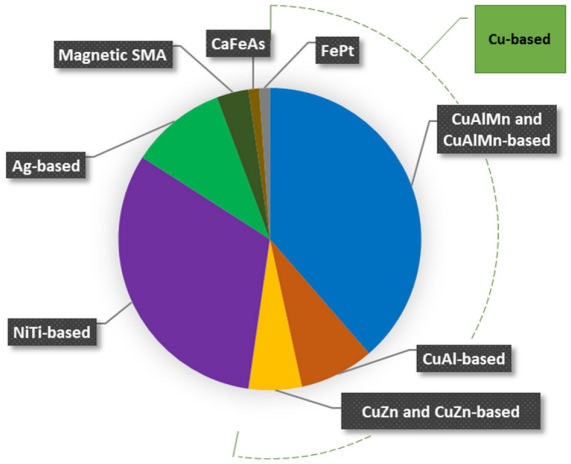


Figure 6. Pie chart representing the percentage of studied cryogenic SMA grouped according to the elemental composition.

Figure 7 lists the revised papers grouped according to the chemical composition and ordered according to their Ms temperature. It is worth underlining that only a few works report the complete quartet of phase transformation temperatures, since very advanced instrumentations are required to achieve temperatures beyond the temperature of liquid nitrogen. For this motivation, the M_f temperature is hardly measurable when TMT is located at cryogenic temperatures. Consequently, the temperatures that identify the reverse TMT (A_s and A_f) are not often reported. Therefore, the M_s temperature has been selected as the key parameter guiding the classification of materials as it has always been the most easily measurable temperature for TMT.

Figure 7 shows that the cryogenic SMA can be grouped into four classes. The first class (I), from 200 to 250 K, contains the greater part of the cryogenic SMA families which can be considered as low-temperature SMA. The second class (II), from 150 to 200 K, is mainly composed of NiTi-based and CuAlMn-based SMA. The alloys of class II can be denoted as low-cryogenic SMA. The third class (III), from 125 to 150 K, is composed of the greater part of cryogenic SMA, similarly to class I. The alloys of class III can be denoted as high-cryogenic SMA. Finally, the fourth class (IV), with the exception of the NiTiHf alloy by Umale et al. [45], consists only of the CuAlMn-based systems. These alloys can be considered as extreme-cryogenic SMA.

Further evidence in the literature on cryogenic SMA is the missing characterization of the typical properties of this class of materials. As stated in the introduction, these materials are mainly considered for their peculiar SME and PE behaviors, so thermomechanical analyses are at the basis of their study and development. For cryogenic SMA involving low temperatures, the collection of such information is extremely challenging; as a consequence, mechanical characterizations are available only for those alloys with higher M_s, where commercial instruments can manage the measurements. This aspect can explain why, despite the homogeneous time distribution of the literature on this subject—supporting evidence for the interest of the scientific community—the resulting development is mainly focused on the material's structural and thermal characteristics, still far from the needs for technological impact.

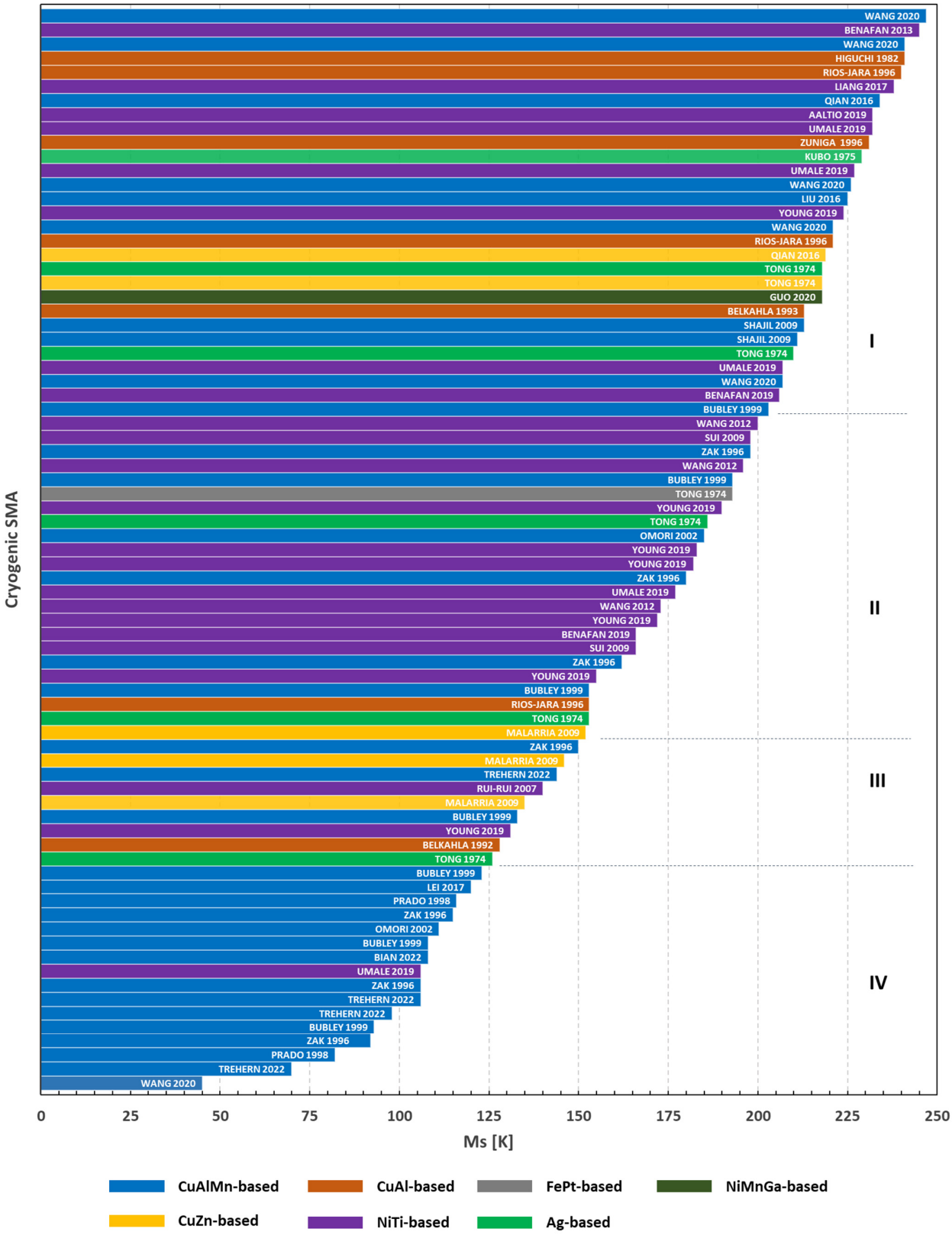


Figure 7. Diagram of the most relevant published cryogenic SMA as a function of their M_s temperature [15–22,25–28,30,32–36,38,40,42–47,50]. Each bar represents a SMA system; inside the bar is the first author of the related paper and year of its publication. I: low-temperature SMA; II low-cryogenic SMA; III: high-cryogenic SMA; IV: extreme-cryogenic SMA.

Another critical issue emerging from this literature review is the strong dependence of the transformation temperature on the alloy composition. This aspect involves a relevant constraint in the alloy composition control, an issue which limits the synthesis strategies and an issue for the upscaling of material production.

Despite the cryogenic applications not being widely diffused in common life, the perspectives associated with the cryocooling technologies, based on He-free solutions and on cheaper cooling liquids, and with advanced heat pumping systems, could represent a further opportunity for the use of these SMA as active components. Such an opportunity is already a reality in some limited fields of application, such as space technologies. Here, the low temperatures involved in the environment suggest the development of active systems based on cryogenic SMA to support specific needs related to mechanical actuation, active damping, or structural requirements.

8. Conclusions

This work is aimed at presenting a review of SMA with phase transformation at cryogenic temperatures and being a guide for future research on this topic. In particular, four main cryogenic regions have been identified, within which are distributed the seven alloy families considered. Due to the observed component-dependent distribution, the four cryogenic regions could be used to choose the optimal alloy for a specific application.

In particular, it has been noted that the Cu-based systems are those most studied. The extensive studies on CuAlMn alloys permitted a critical overview of these materials, suggesting new paths for future works, such as the Mn content higher than 13 wt.%, the Al content lower than 8 wt.%, and the Mn/Al ratio higher than 1.5. In fact, the transition temperature turns out to be drastically affected by the stoichiometries of Mn and Al in the alloy. The addition of a quaternary element does not seem to affect the phase transformation temperatures in this system.

Besides the CuAlMn system, due to the low M_s, cryogenic SMA such as the AgCd system seem attractive for future research presenting TMT in a small concentration range, close to equiatomic composition. A few works dated back to almost 50 years ago suggest that the current characterization techniques could be of great help in redesigning this type of alloy. However, the elements involved are expensive, and for Cadmium, they are also toxic and carcinogenic. Therefore, this system loses all interest with respect to application development.

Finally, opportunities for new findings can also be attained through NiTi-based alloys. The addition of a ternary and/or a quaternary element to NiTi can be accomplished with full knowledge of the cause, with NiTi being the most known SMA. Based on the above-presented works, it is suggested that NiTiHf is the most promising cryogenic NiTi-based SMA, thanks to its low costs, remarkable shape memory and superelasticity, and superior stability, even in low temperature applications

In all the cases, next to the materials' further development, the literature suggests the need for the parallel growth of testing systems in order to characterize and analyze the materials' performance and behavior. Such a step forward will also provide the opportunity to discover other peculiar characteristics of these materials directly related to cryogenic temperatures.

Author Contributions: Conceptualization, C.F. and A.N.; methodology, A.N.; formal analysis, A.N., D.N. and C.F.; investigation, A.N., D.N. and C.F.; data curation, A.N., D.N. and C.F.; writing—original draft preparation, A.N., D.N. and C.F.; writing—review and editing, A.N., D.N. and C.F.; visualization, A.N., D.N. and C.F.; supervision, A.N. All authors have read and agreed to the published version of the manuscript.

Funding: This research received no external funding.

Data Availability Statement: Data sharing not applicable.

Conflicts of Interest: The authors declare no conflict of interest.

References

1. Otsuka, K.; Ren, X. Physical metallurgy of Ti–Ni-based shape memory alloys. *Prog. Mater. Sci.* **2005**, *50*, 511–678. [CrossRef]
2. Nespoli, A.; Besseghini, S.; Pittaccio, S.; Villa, E.; Viscuso, S. The high potential of shape memory alloys in developing miniature mechanical devices: A review on shape memory alloy mini-actuators. *Sens. Actuators A Phys.* **2010**, *158*, 149–160. [CrossRef]
3. Shreekrishna, S.; Nachimuthu, R.; Nair, V.S. A review on shape memory alloys and their prominence in automotive technology. *J. Intell. Mater. Syst. Struct.* **2023**, *34*, 499–524. [CrossRef]
4. Dana, A.; Vollach, S.; Shilo, D. Use the Force: Review of High-Rate Actuation of Shape Memory Alloys. *Actuators* **2021**, *10*, 140. [CrossRef]
5. Nespoli, A.; Biffi, C.A.; Casati, R.; Passaretti, F.; Tuissi, A.; Villa, E. New developments on mini/micro shape memory actuators. In *Smart Actuation and Sensing Systems—Recent Advances and Future Challenges*; Berselli, G., Vertechy, R., Vassura, G., Eds.; IntechOpen Limited: London, UK, 2012; pp. 35–52. [CrossRef]
6. Casagrande, L.; Villa, E.; Nespoli, A.; Occhiuzzi, A.; Bonati, A.; Auricchio, F. Innovative dampers as floor isolation systems for seismically-retrofit multi-storey critical facilities. *Eng. Struct.* **2019**, *201*, 109772. [CrossRef]
7. Saedi, S.; Acar, E.; Raji, H.; Saghaian, S.E.; Mirsayar, M. Energy damping in shape memory alloys: A review. *J. Alloys Compd.* **2023**, *956*, 170286. [CrossRef]
8. Patil, R.A.; Rane, S.B.; Kumbhar, S.B. Investigation of the damping behavior of shape memory alloy-nitinol reinforced composite. *Eng. Res. Express* **2022**, *4*, 045018. [CrossRef]
9. Concilio, A.; Antonucci, V.; Auricchio, F.; Lecce, L.; Sacco, E. *Shape Memory Alloy Engineering for Aerospace, Structural and Biomedical Applications*; Butterworth—Heinemann: Oxford, UK; Elsevier Ltd.: Amsterdam, The Netherlands, 2021. [CrossRef]
10. Wen, C.; Yu, X.; Zeng, W.; Zhao, S.; Wang, L.; Wan, G.; Huang, S.; Grover, H.; Chen, Z. Mechanical behaviors and biomedical applications of shape memory materials: A review. *AIMS Mater. Sci.* **2018**, *5*, 559–560. [CrossRef]
11. Nespoli, A.; Dallolio, V.; Villa, E.; Passaretti, F. A new design of a Nitinol ring-like wire for suturing in deep surgical field. *Mater. Sci. Eng. C* **2015**, *56*, 30–36. [CrossRef]
12. Barbarino, S.; Saavedra Flores, E.I.; Ajaj, R.M.; Dayyani, I.; Friswell, M.I. A review on shape memory alloys with applications to morphing aircraft. *Smart Mater. Struct.* **2014**, *23*, 55175494. [CrossRef]
13. Borlandelli, E.; Scarselli, D.; Nespoli, A.; Rigamonti, D.; Bettini, P.; Morandini, M.; Villa, E.; Sala, G.; Quadrio, M. Design and experimental characterization of a NiTi-based, high-frequency, centripetal peristaltic actuator. *Smart Mater. Struct.* **2015**, *24*, 035008. [CrossRef]
14. Chen, Q.F.; Zuo, X.B.; Wang, L.M.; Chang, W.; Tian, W.Y.; Li, A.Q.; Yang, H.; Liu, L.H. NiTi wire as a superelastic damping material in structural engineering. *Mater. Sci. Eng. A* **2006**, *438–440*, 1089–1092. [CrossRef]
15. Tong, H.C.; Wayman, C.M. Characteristic temperatures and other properties of thermoelastic martensites. *Acta Metall.* **1974**, *22*, 887–896. [CrossRef]
16. Trehern, W.; Ozcan, H.; Franco, B.; Hite, N.; Malone, N.; Loveall, B.; Morrison, T.D.; Benafan, O.; Karaman, I. Exploring thermomechanical functionality of CuAlMn as an extreme low temperature shape memory alloys. *Mater. Lett.* **2022**, *308*, 131246. [CrossRef]
17. Bian, Z.; Song, J.; Liu, P.; Wan, F.; Lei, Y.; Wang, Q.; Yang, S.; Zhan, Q.; Chen, L.; Wang, J. In Situ Observation of Thermoelastic Martensitic Transformation of Cu-Al-Mn Cryogenic Shape Memory Alloy with Compressive Stress. *Materials* **2022**, *15*, 3794. [CrossRef] [PubMed]
18. Zak, G.; Kneissl, A.C.; Zatulskij, G. Shape memory effect in cryogenic Cu–Al–Mn alloys. *Scr. Mater.* **1996**, *34*, 363–367. [CrossRef]
19. Prado, M.O.; Lovey, F.C.; Civale, L. Magnetic properties of Cu–Mn–Al alloys with shape memory effect. *Acta Mater.* **1998**, *46*, 137–147. [CrossRef]
20. Bubley, I.R.; Koval, Y.N.; Titov, P.V. $\beta 1 \rightarrow \gamma'$ transformation in Cu–Mn–Al alloys after low temperature aging. *Scr. Mater.* **1999**, *41*, 637–641. [CrossRef]
21. Omori, T.; Wang, J.; Sutou, Y.; Kainuma, R.; Ishida, K. Two-way shape memory effect induced by bending deformation in ductile Cu-Al-Mn alloys. *Mater. Trans.* **2002**, *43*, 1676–1683. [CrossRef]
22. Shajil, N.; Das, D.; Chandrasekaran, L. Effects of cycling on the pseudoelastic properties of CuAlMnNi & TiNi based pseudoelastic alloys. *Int. J. Struct. Changes Solids Mech. Appl.* **2009**, *1*, 171–185.
23. Niitsu, K.; Omori, T.; Kainuma, R. Superelasticity at Low Temperatures in Cu-17Al-15Mn (at%) Shape Memory Alloy. *Mater. Trans.* **2011**, *52*, 1713–1715. [CrossRef]
24. Niitsu, K.; Kimura, Y.; Omori, T.; Kainuma, R. Cryogenic superelasticity with large elastocaloric effect. *NPG Asia Mater.* **2018**, *10*, e457. [CrossRef]
25. Qian, S.; Geng, Y.; Wang, Y.; Pillsbury, T.E.; Hada, Y.; Yamaguchi, Y.; Fujimoto, K.; Hwang, Y.; Radermacher, R.; Cui, J.; et al. Elastocaloric effect in CuAlZn and CuAlMn shape memory alloys under compression. *Philos. Trans. R. Soc. A* **2016**, *374*, 20150309. [CrossRef]
26. Liu, J.; Huang, H.; Xie, J. Effects of aging treatment on the microstructure and superelasticity of columnar-grained Cu71Al18Mn11 shape memory alloy. *Int. J. Miner. Metall. Mater.* **2016**, *23*, 1157. [CrossRef]
27. Lei, Y.; Qin, X.; Wan, F.; Liu, P.; Chen, L.; Wang, J. In-situ observation of martensitic transformation in Cu–Al–Mn cryogenic shape memory alloys. *Fusion Eng. Des.* **2017**, *125*, 603–607. [CrossRef]

28. Wang, H.; Huang, H.Y.; Su, Y.J. Tuning the operation temperature window of the elastocaloric effect in Cu–Al–Mn shape memory alloys by composition design. *J. Alloys Compd.* **2020**, *828*, 154265. [CrossRef]
29. Zheng, Y.; Li, C.; Wan, F.; Long, Y. Cu–Al–Mn alloy with shape memory effect at low temperature. *J. Alloys Compd.* **2007**, *441*, 317–322. [CrossRef]
30. Malarría, J.; Lovey, F.C.; Sade, M. Two way shape memory effect in CuZnAl single crystals after pseudoelastic cycling at low temperatures. *Mater. Sci. Eng. A* **2009**, *517*, 118–124. [CrossRef]
31. Cisse, C.; Zaeem, M.A. An Asymmetric Elasto-Plastic Phase-Field Model for Shape Memory Effect, Pseudoelasticity and Thermomechanical Training in Polycrystalline Shape Memory Alloys. *Acta Mater.* **2020**, *201*, 580–595. [CrossRef]
32. Belkahla, S.; Zufiiga, H.F.; Guenin, G. Elaboration and characterization of new low temperature shape memory Cu–Al–Be alloys. *Mater. Sci. Eng. A* **1993**, *169*, 119–124. [CrossRef]
33. Higuchi, A.; Suzuki, K.; Matsumoto, Y.; Sugimoto, K.; Komatsu, S.; Nakamura, Y. Shape Memory Effect in Cu–Al–Be Ternary Alloys. *J. Phys. Colloq.* **1982**, *437*, 767–772. [CrossRef]
34. Zuñiga, H.F.; Jara, D.R.; Belkahla, S. The Training and Re-Training Procedures for the Two Way Memory Effect and Its Degradation In A Cu-Al-Be Alloy. *Scr. Mater.* **1996**, *34*, 1899–1904. [CrossRef]
35. Rios-Jara, D.; Planes, A.; Manosa, L.; Ortin, J.; Belkahla, S.; Morin, M.; Guenin, G.; Macqueron, J.L. Martensitic Transition Entropy Ciiange and Elastic Constants of Cu–Al–Be Alloys. *J. Phys. IV* **1991**, *1*, 283–288. [CrossRef]
36. Benafan, O.; Notardonato, W.U.; Meneghelli, B.J.; Vaidyanathan, R. Design and development of a shape memory alloy activated heat pipe-based thermal switch. *Smart Mater. Struct.* **2013**, *22*, 105017. [CrossRef]
37. Krishnan, V.B.; Bewerse, C.; Notardonato, W.U.; Vaidyanathan, R. A thermal conduction switch based on low hysteresis NiTiFe shape memory alloy helical springs. *AIP Conf. Proc.* **2008**, *986*, 3. [CrossRef]
38. Aaltio, I.; Fukuda, T.; Kakeshita, T. Elastocaloric cooling and heating using R-phase transformation in hot rolled Ni–Ti–Fe shape memory alloys with 2 and 4 at% Fe content. *J. Alloys Compd.* **2019**, *780*, 930–936. [CrossRef]
39. Liang, Y.; Jiang, S.; Zhang, Y.; Yu, J. Microstructure, Mechanical Property, and Phase Transformation of Quaternary NiTiFeNb and NiTiFeTa Shape Memory Alloys. *Metals* **2017**, *7*, 309. [CrossRef]
40. Jing, R.-R.; Liu, F.-S. The Influence of Co Addition on Phase Transformation Behavior and Mechanical Properties of TiNi Alloys. *Chin. J. Aeronaut.* **2007**, *20*, 153–156. [CrossRef]
41. Dang, P.; Zhang, L.; Zhou, Y.; Liang, Q.; Ding, X.; Sun, J.; Xue, D. Cryogenic Superelasticity and Elastocaloric Effect in a Nanostructured Ti–Ni–Co Alloy. *Scr. Mater.* **2023**, *236*, 115638. [CrossRef]
42. Wang, M.; Jiang, M.; Liao, G.; Guo, S.; Zhao, X. Martensitic transformation involved mechanical behaviors and wide hysteresis of NiTiNb shape memory alloys. *Prog. Nat. Sci. Mater. Int.* **2012**, *22*, 130–138. [CrossRef]
43. Sui, J.H.; Gao, Z.Y.; Li, Y.F.; Zhang, Z.G.; Cai, W. A study on NiTiNbCo shape memory alloy. *Mater. Sci. Eng. A* **2009**, *508*, 33–36. [CrossRef]
44. Benafan, O.; Bigelow, G.S.; Garg, A.; Noebe, R.D. Viable low temperature shape memory alloys based on Ni–Ti–Hf formulations. *Scr. Mater.* **2019**, *164*, 115–120. [CrossRef]
45. Umale, T.; Salas, D.; Tomes, B.; Arroyave, R.; Karaman, I. The effects of wide range of compositional changes on the martensitic transformation characteristics of NiTiHf shape memory alloys. *Scr. Mater.* **2019**, *161*, 78–83. [CrossRef]
46. Young, A.W.; Torgerson, T.; Ley, N.A.; Gomez, K.; Benafan, O.; Young, M.L. Effects of Sn Addition on NiTi Shape Memory Alloys. *Shape Mem. Superelast.* **2019**, *5*, 125–135. [CrossRef]
47. Kubo, H.; Hamabe, A.; Shimizu, K. Thermoelastic martensitic transformation and associated shape memory effect in a Ag–Al alloy. *Scr. Metall.* **1974**, *9*, 1083–1087. [CrossRef]
48. Prasad, K.V.S.; Bansal, C. Resistivity and Thermoelectric Power Measurements on AgCd Shape Memory Alloys. *Phys. Stat. Sol.* **1986**, *98*, 453–465. [CrossRef]
49. Sypek, J.T.; Yu, H.; Dusoe, K.J.; Drachuck, G.; Patel, H.; Giroux, A.M.; Goldman, A.I.; Kreyssig, A.; Canfield, P.C.; Bud'ko, S.L.; et al. Superelasticity and cryogenic linear shape memory effects of $CaFe_2As_2$. *Nat. Commun.* **2017**, *8*, 1083. [CrossRef]
50. Guo, J.; Wei, Z.; Shen, Y.; Zhang, Y.; Li, J.; Hou, X.; Liu, J. Low-temperature superelasticity and elastocaloric effect in textured Ni–Mn–Ga–Cu shape memory alloys. *Scr. Mater.* **2020**, *185*, 56–60. [CrossRef]
51. Niitsu, K.; Xu, X.; Umetsu, R.Y.; Kainuma, R. Stress-induced transformations at low temperatures in a $Ni_{45}Co_5Mn_{36}In_{14}$ metamagnetic shape memory alloy. *Appl. Phys. Lett.* **2013**, *103*, 242406. [CrossRef]

Disclaimer/Publisher's Note: The statements, opinions and data contained in all publications are solely those of the individual author(s) and contributor(s) and not of MDPI and/or the editor(s). MDPI and/or the editor(s) disclaim responsibility for any injury to people or property resulting from any ideas, methods, instructions or products referred to in the content.